Zhiren Wang

M. Sc. in Micro and Nanotechnologies for Integrated Systems

2015 - 2017

ETH Zurich

Development of Sputtering Process for High Quality Nb Thin Film

01.03.2017 - 31.08.2017

Project supervisor:

Andreas Wallraff – andreas.wallraff@phys.ethz.ch
Anton Potočnik – anton.potocnik@phys.ethz.ch

Phelma tutor:

Ouisse Thierry – thierry.ouisse@grenoble-inp.fr

Ecole nationale supérieure de physique, électronique, matériaux

Phelma
Bât. Grenoble INP - Minatec
3 Parvis Louis Néel - CS 50257
F-38016 Grenoble Cedex 01

Tel +33 (0)4 56 52 91 00
Fax +33 (0)4 56 52 91 03

http://phelma.grenoble-inp.fr

Eidgenössische Technische Hochschule Zürich

ETH Zürich
Rämistrasse 101
8092 Zürich
Switzerland

Tel +41 44 632 1111

https://www.ethz.ch

Abstract

In this thesis a detailed investigation of Nb thin film deposition has been conducted using the AJA dual-chamber sputtering equipment. The process has been successfully optimized for achieving a high quality 150 nm Nb thin films. To optimize the process, five important parameters have been studied: target-substrate distance, target power, RF bias power and substrate temperature. The thin film is characterized by a variety of techniques such as resistivity, film thickness, topography, surface roughness, stress, superconducting critical temperature and temperature dependent resistivity. As a result, the best film quality was obtained with the deposition at the highest rate (0.85 nm/s), 2 mTorr Ar gas pressure, zero RF bias, substrate temperature of 600°C, 650 W target DC power and 130 mm substrate-target distance. The best film parameters have shown a critical temperature (T_c) of 9.34 K and residual resistivity ratio (RRR) of 40.

Dans cette thèse, une recherche approfondie du dépôt de couche minces de Nb a été effectuée en utilisant la système de pulvérisation en double chambres de la compagnie AJA. Le processus a été optimisé avec succès pour réaliser des couches minces de Nb de 150 nm de haute qualité. Pour optimiser le processus, cinq paramètres importants ont été étudiés: la distance cible-substrat, la puissance de cible, la puissance de biais RF, la pression du gaz et la température du substrat. La couche mince est caractérisée par plusieurs techniques telles que la résistivité, l'épaisseur, la topographie, la rugosité de surface, le stress, la température critique du supraconducteur et la dependence en temperature de la résistivité. Par conséquent, la meilleure qualité de couche mince de Nb a été obtenue avec le taux de dépôt le plus élevé (0.85 nm/s), une pression gazeuse d'argon de 2 mTorr, sans biais RF, une température de substrat de 600°C, une puissance de cible de 650 W et une distance cible-substrat de 130 mm. Les meilleurs paramètres de couche ont une température critique (T_c) de 9.34 K et un ratio de résistivité résiduelle (RRR) de 40.

In questa tesi una ricerca approfondita della deposizione di film sottili di Nb è stata effettuata usando un sistema di sputtering a doppia camera dell' azienda AJA. Il processo è stato ottimizzato per produrre film sottili di alta qualità e spessore 150 nm. Per ottimizzare il processo, cinque parametri importanti sono stati studiati: la distanza del target dal substrato, la potenza applicata al target, la potenza della polarizzazione RF, la pressione del gas e la temperatura del substrato. La caratterizzazione del film è basata su parametri come la resistività, lo spessore, la topografia, la rugosità della superficie, lo stress, la temperatura critica del superconduttore e la dipendenza dalla temperatura della resistività. I film di migliore qualità sono stati ottenuti con il più alto tasso di deposizione (0.85 nm/s), 2 mTorr di pressione di argon nella camera di deposizione, senza polarizzazione RF, con una temperatura del

substrato di 600°C, una potenza sul target di 650 W e una distanza target-substrato di 130 mm. Questi film hanno una temperatura critica (T_c) di 9.34 K e un rapporto resistività residua (RRR) di 40.

Contents

Chapter 1

Introduction

The history and concept of quantum computing can be dated back to Richard Feynman's idea of simulating a quantum system with quantum computer in 1982. The basic building block for a quantum computer is called a "qubit", which plays a similar role as its counterpart "bit" in classical computers. There are several cancidates for the physical realization of a quantum computer, such as single photons [1], trapped ions [2], nuclear magnetic resonance [3], quantum dots [4] and superconducting circuits [5, 6]. Nowadays, superconducting circuits are among the most promising candidates for building a quantum computer [7] due to ultra-low dissipation and with that long coherence times [8], ultra-low noise and high measurement precision, strong and tunable nonlinearity [9], and potential for scalability using design and fabrication techniques similar to those developed in standard semiconductor integrated circuits.

However, the main obstacle for building a quantum computer is to maintain quantum information and coherence sufficiently long, so that the implemented quantum gates and algorithms work with high fidelity [10]. Long coherence times are related to low losses in the circuit, chracterized by energy relaxation time T_1,

$$\frac{1}{T_1} = \frac{\omega}{Q} \tag{1.1}$$

where Q is the quality factor of the circuit and ω is the circuit's resonant frequency [11]. Quality factor is a value to characterize the loss level of a resonant circuit. To realize circuits with long coherence times, high quality factors are needed.

In superconducting circuits one of the basic elements is a resonator. Resonator plays an important role for circuit quantum electrodynamics (Circuit QED) architecture and can be used as qubit readout [12] or radiation detector [13]. In the resonators, the origin of circuit losses are defects and impurities at the interfaces [14,15], including Metal-Substrate (MS), Metal-Vacuum (MV), Substrate-Vacuum (SV), as shown in Figure 1.1. MS is one of the dominant interfaces among these three. Therefore there is the need for developing a deposition process which would give high quality metal thin film and clean interface in order to realize a high-Q resonator.

There is variety of choices for the superconducting materials used for superconducting circuits, such as Al, Nb, NbN, TiN, NbTiN, where the most popular ones are Nb and Al. The substrate can be either high resistance Si or sapphire (Al_2O_3). Niobium is particularly interesting since its high critical temperature (9.4 K) [16]

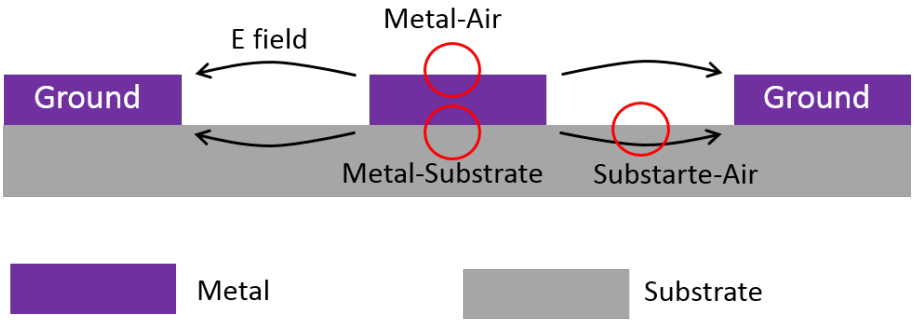

Figure 1.1: The schematic of the intersection of a CPW resonator, where the three interfaces are the origin of circuit losses and metal-substrate interface is the dominant one.

allows the circuit to be characterized at liquid helium temperature. To build a resonator with high quality factor, a high quality Nb thin film is needed.

In this thesis, the deposition of high quality Nb thin films on Al_2O_3 substrate is investigated by using DC magnetron sputtering technique in a ultra high vacuum (UHV) chamber. Five critical process parameters have been studied: target-substrate distance, target power, RF bias power, Ar gas pressure and substrate temperature. Several characterization techniques are used to study the results from the deposition process, including resistivity, thickness, superconducting critical temperature, stress, surface roughness and residual resistivity ratio (RRR). The goal is to find out the optimal process parameters giving the best Nb thin film quality.

Chapter 2

Superconductivity

The phenomenon of superconductivity was discovered in 1911 by H. Kamerlingh Onnes [17]. He observed that the electrical resistance of mercury disappeared completely below a critical temperature T_c. The perfect conductivity or zero resistance below T_c is one of the key characteristics of superconductors. The theory that explains this phenomenon is the BCS theory [18]. When the temperature is below T_c electrons are paired by electron-phonon interaction and form so-called Cooper pairs. Cooper pairs without being scattered which leads to zero resistance. This property allows us to determine T_c by measuring resistance.

Another important characteristic of superconductor is called "Meissner effect", discovered by Meissner and Ochsenfeld in 1933 [19]. The bulk superconductor shows perfect diamagnetism when temperature is cooled below T_c. The magnetic flux will be expelled when the metal transits from normal state to superconducting state. However, at the edge of the superconductor, the magnetic field penetrates the metal within a finite distance λ, called London penetration depth [20]. London penetration depth $\lambda_L(T)$ is temperature dependent and at zero temperature it is defined in equation 2.1.

$$\lambda_L(0) = \sqrt{\frac{m_e}{n_s(0)e^2\mu_0}}, \tag{2.1}$$

where m_e is the mass of an electron, e is the elementary charge, $n_s(0)$ is the density of superconducting electrons and μ_0 is the vacuum magnetic permeability.

For large applied magnetic fields above critibal field H_c, the superconductivity is destroyed. The temperature dependence of H_c can be approximated as equation [8]:

$$H_c(T) = H_c(0)\left[1 - \left(\frac{T}{T_c}\right)^2\right] \tag{2.2}$$

The temperature dependence of the critical field is shown in Figure 2.1. When the magnetic field is small ($H \ll H_c$), the T_c reduces with H in an approximate linear dependence.

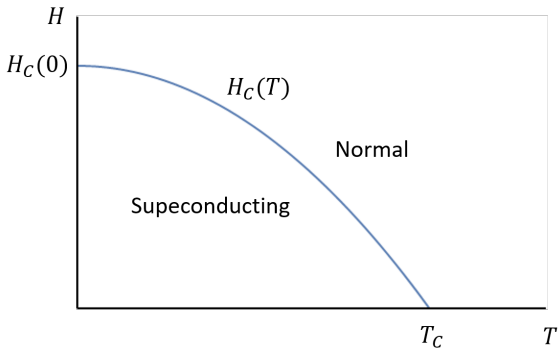

Figure 2.1: Temperature dependence of the critical field. The curve separates the normal state and superconducting state.

Chapter 3

Niobium Thin Film Deposition

3.1 Deposition Techniques for Niobium Thin Films

In general, the technique used for metal thin film deposition is called Physical Vapour Deposition (PVD). There are two major types of PVD techniques: thermal evaporation and sputtering. In the evaporation technique metal vapour is generated by heating the metal target and then deposited on the wafer, while in sputtering tool instead of high temperature the plasma is utilized to bombard the metal target and generate free metal atoms, which are then deposited on the substrate surface. In practice, the preferred technique for Nb deposition is sputtering, since its high melting point (2750 K) makes it difficult to use in evaporator.

In this thesis Nb is deposited by using sputtering machine AJA ATC2200C from AJA Inc., as shown in Figure 3.2. The equipment contains three chambers: load lock (LL) for loading the sample, oxidation high vacuum (HV) chamber and main ultra high vacuum (UHV) chamber. In our experiments, all the steps are done in the UHV chamber, where the pressure was around 5×10^{-8} Torr.

Inside the UHV chamber, there are eight different metal targets as shown in Figure 3.1, including Ti, Al, Nb. The Nb target used in our experiments is a 4-inch target placed in the central gun.

3.2 Sputtering Process for Nb thin films

The metal deposition process starts with a clean sapphire wafer. Firstly, either diced chips or a wafer is clamped on a sample holder as shown in Figure 3.3 and loaded to the load lock. When the load lock pressure reaches below 10^{-7} Torr, the gate valve between the load lock and the HV chamber is opened. The sample holder is transferred from load lock to the HV chamber with a transfer arm. A propeller in the HV chamber is lowered down and fixes the sample holder so that the sample holder can be lifted up from the transfer arm. The transfer arm is then pulled back to the load lock and the gate is closed. At this point, the gate between the HV and the UHV chamber is opened. The sample holder is transferred from the HV to the UHV chamber with a second transfer arm and attached to the UHV chamber's propeller. After the wafer holder height is adjusted and the gate between the HV and UHV chamber is closed, the wafer is ready for the deposition process.

In the beginning of the process, the valve of cryo pump is closed and Ar gas is released with a flow of 30 sccm (Standard Cubic Centimeter per Minute). The

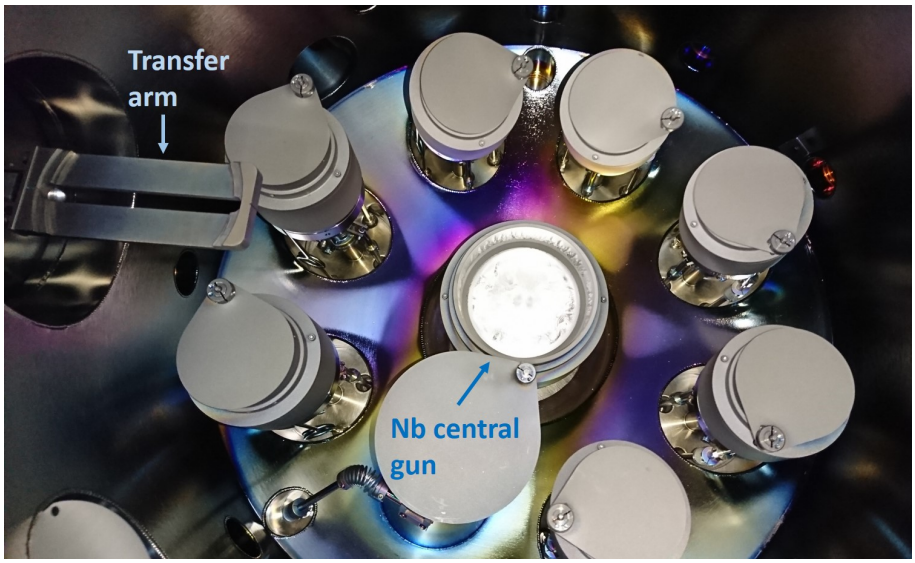

Figure 3.1: The target guns inside UHV chamber. The central Nb gun is used for deposition in this thesis.

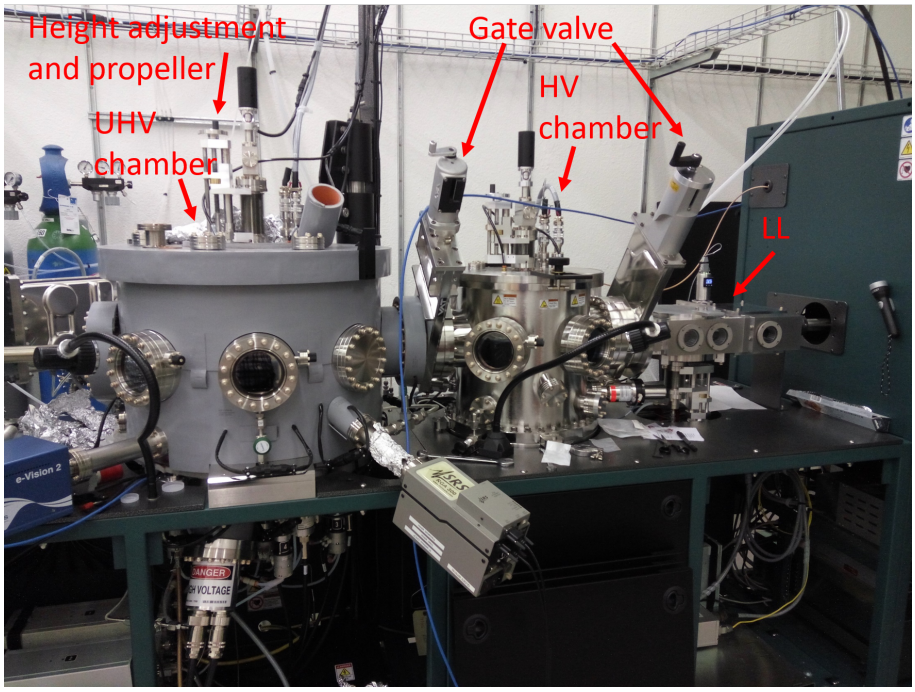

Figure 3.2: The AJA sputtering equipment for Nb deposition, where three chambers are marked in the figure: Ultra High Vacuum (UHV), High Vacuum (HV) and Load Lock (LL). There are two gate valves separating three chambers. The sample holder is fixed by a propeller and its height inside the chamber can be adjusted by a wheel on the top.

pressure of 30 mTorr is chosen for igniting plasma with a 50 W DC power and later reduced to 2 mTorr for process. The DC power then ramps up to the process power in 2 min and is kept for 2 min with the target shutter closed for presputtering. Next step is to open the shutter for a certain coating time. Finally the power ramps down and the target is switched off and the gas valve is closed. When process is finished,

the sample holder is transferred back to load lock. Finally the load lock is vented with N_2.

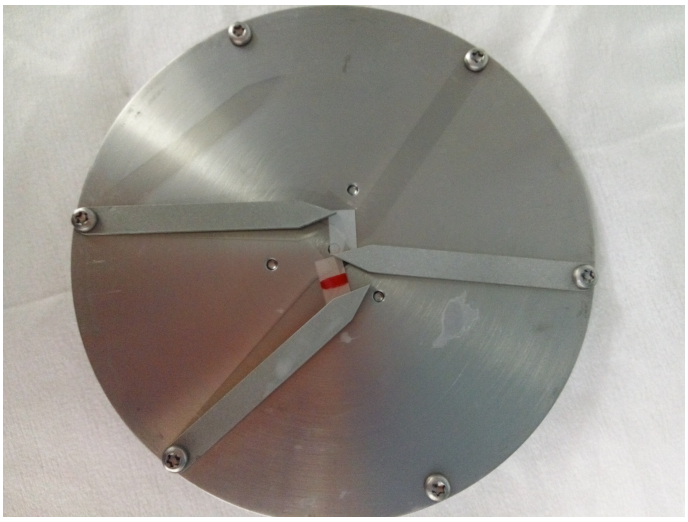

Figure 3.3: Two chips (12 × 6 mm) are clamped on the sample holder.

3.3 Process Parameters

In the sputtering process Ar ions in the plasma bombard the target material. Fragments of the target material fly towards the substrate where they are slowly being deposited (Figure 3.4). We control the film deposition with 5 parameters, which are critical to the deposition of metal film, including distance between sample holder and target, substrate temperature, RF substrate bias, target power, Ar gas pressure. The goal in this process is to achieve the optimal thin film quality (fewer defects and fewer impurities) by studying how these parameters influence the process.

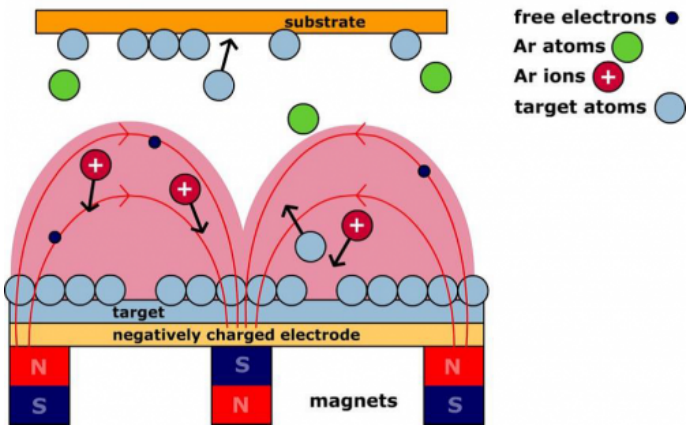

Figure 3.4: The schematic of magnetron sputtering principles. Ar plasma bombards with Nb target and free metal atoms are generated, which coats the surface of the substrate. The magnets below the target localize the plasma and improves bombardment efficiency so that the Ar pressure can be kept at a low pressure (2 mTorr). Taken from [21].

3.3.1 Target-Substrate Distance

In the UHV chamber, the adjustable distance between target and substrate ranges from 130 mm to 230 mm. The deposition rate has inverse square dependence on the distance and the recommended values are between 50 mm and 200 mm (the distance of substrate lowered, measuring from the top).

In addition to the deposition rate, the distance also affects the uniformity of the deposited film. According to the theoretical model in [22], when substrate-target distance d is lower than $0.8R$, where R is the diameter of the metal target, the film has an inferior uniformity. When the substrate is placed farther, the better uniformity will be. The target used in this thesis is a 4-inch (100 mm) central gun, thus the smallest working distance 130 mm is capable to provide a good uniformity.

Therefore we choose the shortest distance to obtain a highest deposition rate so that the process can be finished as fast as possible and least impurities will be in the film.

3.3.2 Target Power

The power supply in sputtering system can be either DC or RF. The DC power provides direct acceleration of ions for bombardment with the target. However, it will not work for insulating target because of zero current flow. Instead, an RF power is applied to make it possible to sputter dielectric materials [23]. Since the material we want to deposit is Nb, the power used in this thesis will be DC power

In the sputtering system, the target power also determines the deposition rate. Larger applied power increases kinetic energy of Ar ions so that the bombardment will be stronger and the deposition rate increases. At the same time, the maximum power is determined by the allowed current density on the target, which varies from one type of material to another. In our system, the highest power on 4-inch Nb target can reach 650 W.

To achieve the highest deposition rate, we apply the maximum allowed 650 W power.

3.3.3 RF Substrate Bias

In the AJA sputtering system, an RF bias can be applied to the substrate. In this way, the Ar plasma will not only bombard the metal target, but also the substrate, resulting in a more dense film. In addition, RF plasma will repel and reduce impurities in the film.

On the contrary, the presence of Ar bombardment caused by the RF bias disturbs the crystal formation of the Nb, resulting in less crystalline structure. If the RF bias is stronger, the etching effect and redeposition will be enhanced. RF bias can also enhance the incorporation of Ar atom in the Nb film. As a result, the film stress will be high compressive according to literature [24].

3.3.4 Ar Gas Pressure

The Nb sputtering is done with only Ar gas. The purity of Ar gas source will directly determine the impurity level in deposited Nb thin film. The purity level of

Ar is 99.9999 %, but impurities can also be introduced from the gas source and the transfer tubes.

As for the deposition, the pressure of Ar gas affects the stress of the film, as shown in Figure 3.5. Sputtered film contains Ar atoms. Larger Ar content leads to more compressive stress [25]. At low pressure, Ar ions have longer mean free path. When Ar reaches the surface of deposited film, it will be more likely incorporated in the film resulting in compressive stress. When the Ar pressure increases, less Ar content in the film will be and compressive stress reduces. If the pressure keeps increasing, Ar content in the film will increase due to larger probability of Ar incorporation. As a result, the tensile stress reduces [24].

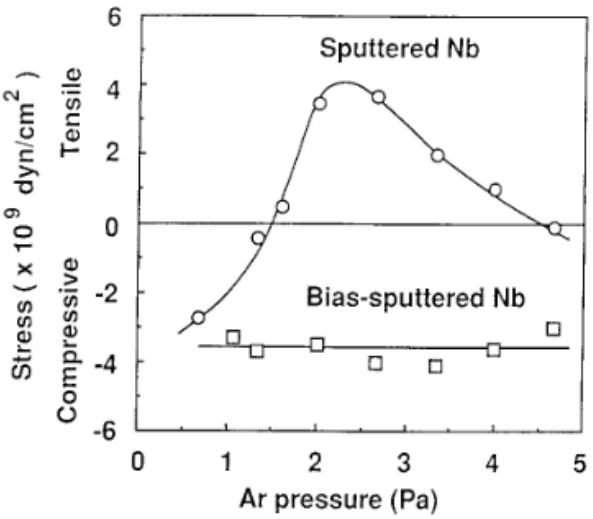

Figure 3.5: Stress of Nb films as a function of Ar pressure during sputtering. Bias voltage is -200 V. Taken from [24]

In our experiment, we choose a relative low pressure (2 mTorr) for deposition and sacrifices stress, considering less impurities and contamination. As a consequence, the film will have highly compressive stress.

3.3.5 Substrate Temperature

Substrate temperature is one of the most important parameters as it can rearrange atoms to form a lattice and reduce defects in the crystal formation. In principle temperatures near the melting point would be needed to successfully rearrange atoms. However, since high temperatures will also affect the substrate lattice and with this disturb the deposition, the optimal deposition temperature has to be found. For Nb on a sapphire substrate there is a temperature window for material growth performed far below the melting point. This window is different according to the melting point of deposited film and substrate.

The typical temperature window for Nb is around 500°C to 700 °C, which means the epitaxial growth can happen for Nb within this window [26].

In our system, the heater can reach a maximum temperature of 1000°C. So the range of in our study will be varied from 25°C to 1000°C with a step of 200°C.

Chapter 4

Film Characterization

In order to investigate the results of deposition, several characterization techniques are used to study the film properties, including resistivity, thickness, critical temperature, stress, surface roughness and residual resistivity ratio (RRR).

4.1 Four-Probe Measurement

4.1.1 Resistivity

Resistivity is one of the most important parameters characterizing the quality of metals and semiconductors. A convenient tool to measure resistivity is the "four-point probe" or "four-probe measurement". Figure 4.1a shows a schematic of the basic experimental setup and the working principles, where t is the film thickness, d is the distance between two adjacent probes and l is the distance from the outer probe to the edge of the sample.

In four-probe tools, the probes are typically placed on a line, where the outer pair is connected to a current source and inner pair measures the voltage difference. Therefore the resistance can be calculated using equation 4.1,

$$R = \frac{V}{I} \tag{4.1}$$

where I and V are the input current and readout voltage respectively. In 4-probe method, the contact resistance is excluded and the measured resistance is therefore of the material under study.

In the case of an infinite sheet, the sheet resistance can be obtained from equation 4.2, only if the probe separation is equidistant [27].

$$R_s = \frac{\pi}{\ln 2}\frac{V}{I} = 4.532\frac{V}{I} \tag{4.2}$$

$$d_{12} = d_{23} = d_{34} = d \tag{4.3}$$

For the finite sheet of material, the infinite situation can be applied as approximation if the following conditions are satisfied [28]:

$$t \leqslant 0.4d \tag{4.4}$$

$$l \geqslant 5d \tag{4.5}$$

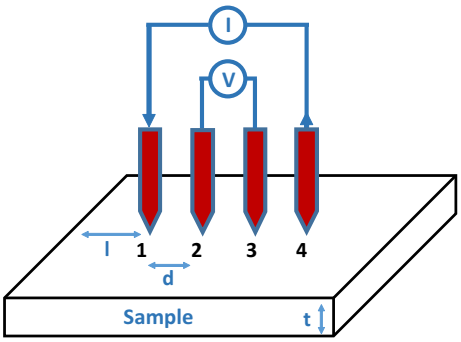

(a)

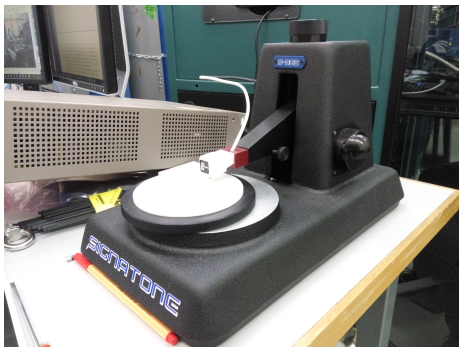

(b)

Figure 4.1: (a) Schematic of a four-probe measurement setup (b) Four-probe station used in this thesis (Signatone S-304)

Where t is the film thickness; d is the probe spacing distance; l is the distance from the edge to the measurement point.

From the sheet resistance, the specific resistivity ρ can be derived from equation 4.6 if the film thickness is known or if the resistivity is known the thickness of the film can be derived.

$$\rho = R_s \cdot t \tag{4.6}$$

The specific resistivity ρ is the inherent property of the material which characterizes the electrical transport of the material. In this work specific resistivity represents one of the important characteristics that measures the quality of the film.

4.1.2 Uniformity

The uniformity of the film is determined from sheet resistance. Figure 4.2 shows an example of measuring the uniformity of the deposited film (Test 1 in deposition rate study, see Section 5.1). The resistance is first measured at different parts of the wafer. Then by using a software Rezist, the resistance can be mapped on the wafer according to the position where the measurement was done. Each small square in Figure 4.2 marks one four-probe measurement. As a result, the average resistance (2-inch range) can be calculated by eliminating the edge values.

As for the uniformity, which can be calculated from Equation 4.7, we have considered both 4-inch case and 2-inch case.

$$\text{Uniformity} = \frac{\text{Max}(R) - \text{Min}(R)}{\bar{R}} \tag{4.7}$$

4.2 Topography and Surface Roughness - Atomic Force Microscope (AFM)

The Atomic Force Microscope (AFM) is widely used characterization technique among Scanning Probe Microscope (SPM) family, which gives information of the surface with atomic resolution [29]. The principle of AFM is based on van der Waals force between atoms or molecules. A sharp tip is mounted at the end of the cantilever. During the scanning of the tip on the material surface, the changing of

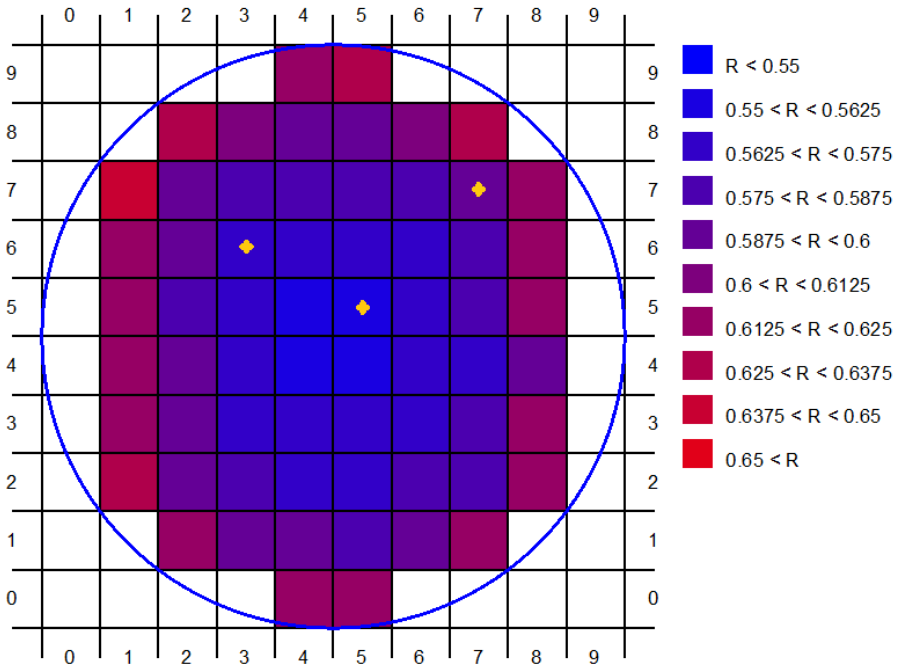

Figure 4.2: Unifomity measurement: Resistance measurements and their position mapping on a 4-inch wafer. Yellow dots mark the point chosen for uniformity calculation of both 4-inch and 2-inch cases. The values in the figure is the direct measurement results from the equipment and the sheet resistance can be derived from equation 4.2

force is reflected by the bending of cantilever and finally magnified and translated into optical signal. The AFM can work in "contact mode" (tip is kept in contact with material during scanning) or "tapping mode" (tip is in continuously tapping the material at a certain frequency).

In this thesis, all the samples are measured in "tapping mode" by the Bruker AFM FastScan, shown in Figure 4.3.

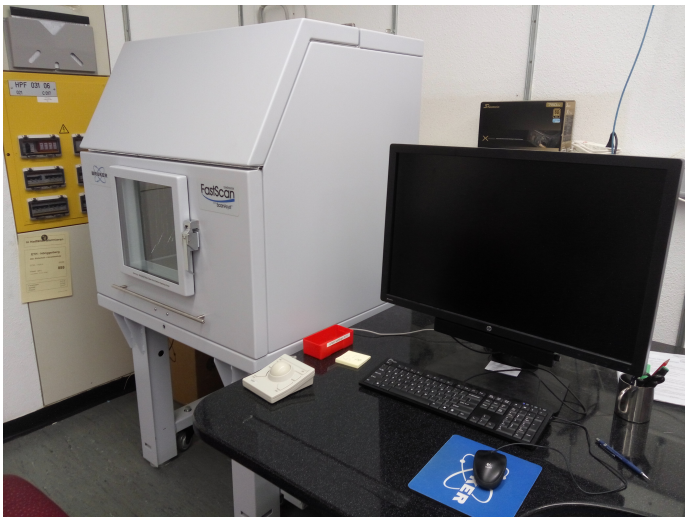

Figure 4.3: The Bruker FastScan AFM equipment

By probing the surface of deposited film, we are able to determine the topogra-

phy and surface roughness of the material, which are related to the quality of the deposited film.

When the 2D scan of surface is measured, the surface roughness is calculated by Root-Mean-Square (RMS) average of height deviation from the mean image plane, as shown in the following equation:

$$R_q = \sqrt{\frac{1}{n}\sum_{i=1}^{n} z_i^2} \tag{4.8}$$

where z_i is the deviation between measured height and mean height for each point in the image, n is the number of points in one image. R_q value defines surface roughness. The higher the R_q is, the rougher the surface will be.

4.3 Thickness Measurement

The sputtering tool used in this thesis has no thickness monitor. Therefore, to determine the thickness we use DektakXT Surface Step Profiler to measure the thickness of deposited film, as shown in Figure 4.4. The tip scans over the surface of the sample across either a trench or a hole. A typical profile can be seen in Figure B.1 in Appendix B, from which film thickness can be obtained.

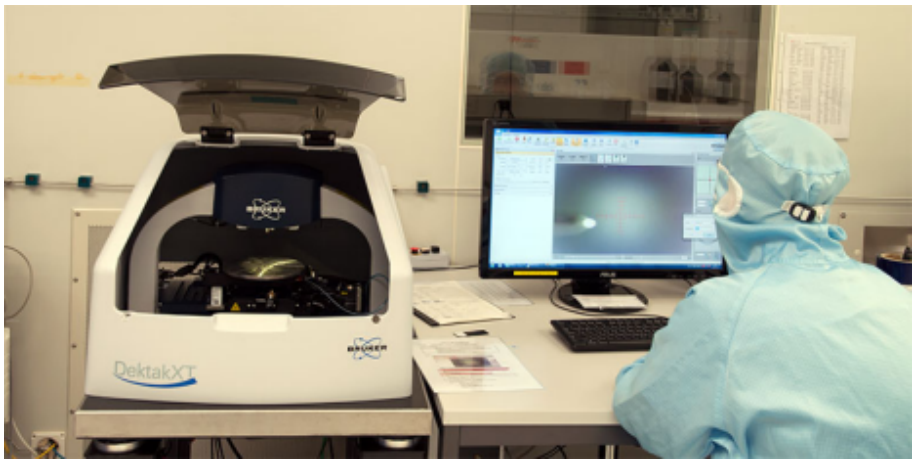

Figure 4.4: The DektakXT Surface Step Profiler is used for measuring film thickness

The trench or hole in the film is done by either using a "lift-off" process or a etching method. For the lift-off process, a marker pen is used to draw a line on the small sample, as shown in Figure 4.5. After metal deposition, this line can be easily removed with acetone and isopropanol in ultrasonic bath. For the sample deposited at high temperatures ($T > 100$ °C), this method is no longer suitable, because of the high temperature decomposition of the chemicals from the marker pen. Instead, an etching process (a calibrated etch recipe in Reactive Ion Etching machine) is used to obtain a trench. Figure B.2 in Appendix B shows the AFM topography of the trench and thickness measurement. Since sapphire is good etch stopping material for fluorine based chemistry in dry etching process and only a few nanometers will be etched away. The error (3 nm) introduced by this method is acceptable for our experiments.

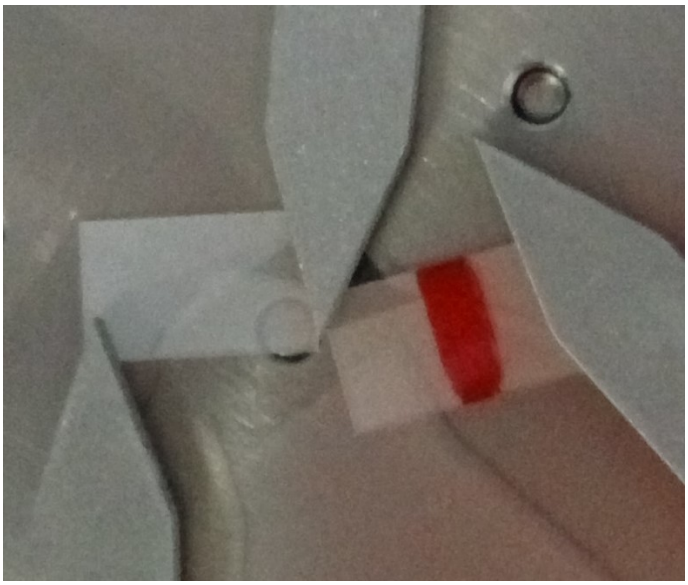

Figure 4.5: Two sapphire chips mounted on the sample holder with three clamps ready for deposition. The red line is used for lift-off process

4.4 Stress Measurement

The Ar pressure and substrate temperature in the sputtering system will influence the stress of the deposited thin film. The stress is measured with Tencor Stressmeter, as shown in Figure 4.6. The stress is obtained from curvature of a thin layer deposited on a wafer, where the change in the radius is measured with a laser reflected from the film surface. Since the two laser sources (670 nm and 780 nm) are not reflected on sapphire wafers, for measuring stress we have deposited thin films on Si wafers.

Figure 4.6: Thin Film Stress Measurement System

4.5 Superconducting Critical Temperature - Magnetic Property Measurement System (MPMS)

Superconducting transition critical temperature (T_c) is one of important parameters of a superconductor. It typically depends on the quality of the superconductor. Impurities and lattice imperfection reduce the critical temperature of the superconductor.

The superconducting state has no resistance and exhibits the Meissner effect, where magnetic field is expeled from the superconducting material [8]. Therefore the transition from normal to superconducting state can be determined by either magnetic moment measurement or electrical resistance measurement. In this thesis T_c measurement is done by both techniques.

Here we will introduce the technique for magnetic susceptibility measurement performed by Magnetic Property Measurement System (MPMS), as shown in Figure 4.7a. The magnetic moment is measured with an internal Superconductor QUantum Interference Device (SQUID) magnetometer.

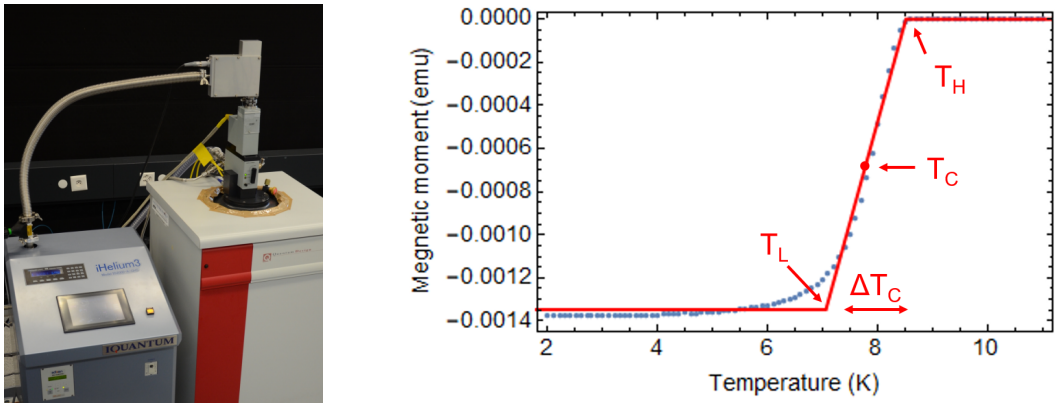

(a) (b)

Figure 4.7: (a) The Magnetic Property Measurement System (MPMS) for T_c measurement. (b) Magnetic moment measurement as a function of temperature for sample deposited at room temperature with a deposition rate of 0.85 nm/s

Before the measurement the sample is cooled down to 2 K in zero magnetic field. Then a finite field is applied and magnetic response is measured as a function of temperature. In the superconducting state, magnetic moment is negative due to perfect diamagnetism ($\chi = -1$) and reduces close to 0 value after the transition to the metallic state, shown in Figure 4.7b. The blue dots are the measured data and the red solid line is the fitted piecewise function composed by three linear functions. The on-set of transition T_H marks the beginning of superconducting transition from the normal state and T_c value is determined as the average of extracted T_H and T_L. The ΔT_c ($\Delta T_c = T_H - T_L$) gives the transition width.

From the MPMS measurement, both the critical temperature T_c and transition width ΔT_c characterize the superconductor. The more homogeneous the film is, the sharper the transition will be. Since T_c decreases with increasing magnetic field, we repeat the measurement for several fields (50 Oe, 100 Oe, 200 Oe and 300 Oe), see Figure 4.8, and take the extrapolated value at $H = 0$, as shown in Figure 4.9.

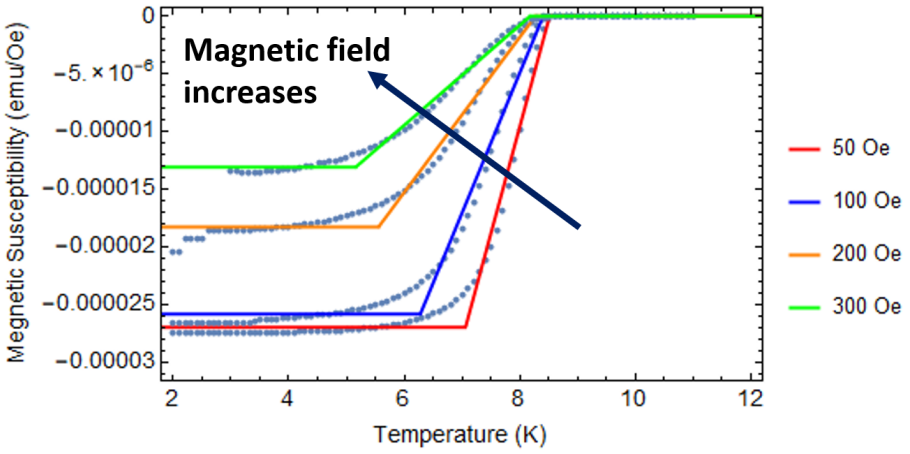

Figure 4.8: The MPMS measurement results for the test with a deposition rate of 0.85 nm/s, see Section 5.1, and fitted function at different applied magnetic field. The transition width ΔT_c broadens when the magnetic field increases.

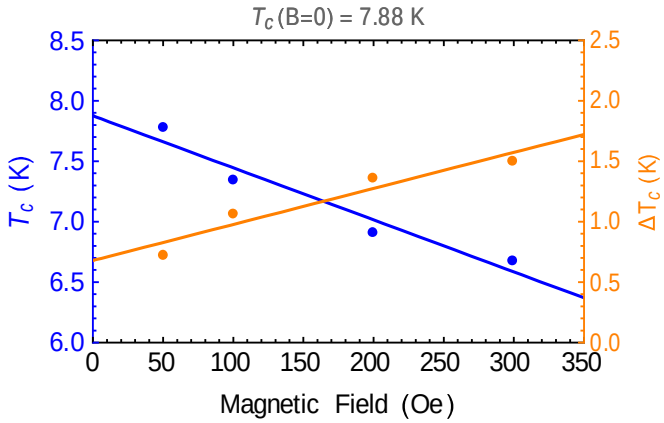

Figure 4.9: The T_c and ΔT_c vs. magnetic field relation and the extraction of T_c at zero field (Deposition rate: 0.85 nm/s). The left Y-axis shows the T_c values at each magnetic field. The right Y-axis shows the corresponding extracted transition width.

4.6 Temperature Dependence Resistance

The parameter that determines the purity of the deposited metal is the Residual Resistivity Ratio (RRR). We determine RRR as a value of resistivity at 10 K and 290 K.

The ratio between resistivity can be obtained from the ratio between resistance directly, as shown in equation 4.9.

$$RRR = \frac{\rho_{290K}}{\rho_{10K}} = \frac{R_{290K}}{R_{10K}} \tag{4.9}$$

The residual resistivity of metal originates from the electron scattering by impurities or defects in the lattice [30]. Therefore, the RRR value is another important factor for benchmarking the quality of a superconductor apart from T_c. With temperature dependent resistance measurement, we also measure T_c of the film. Together with the measurement in MPMS, they provide a more complete investigation

for the T_c.

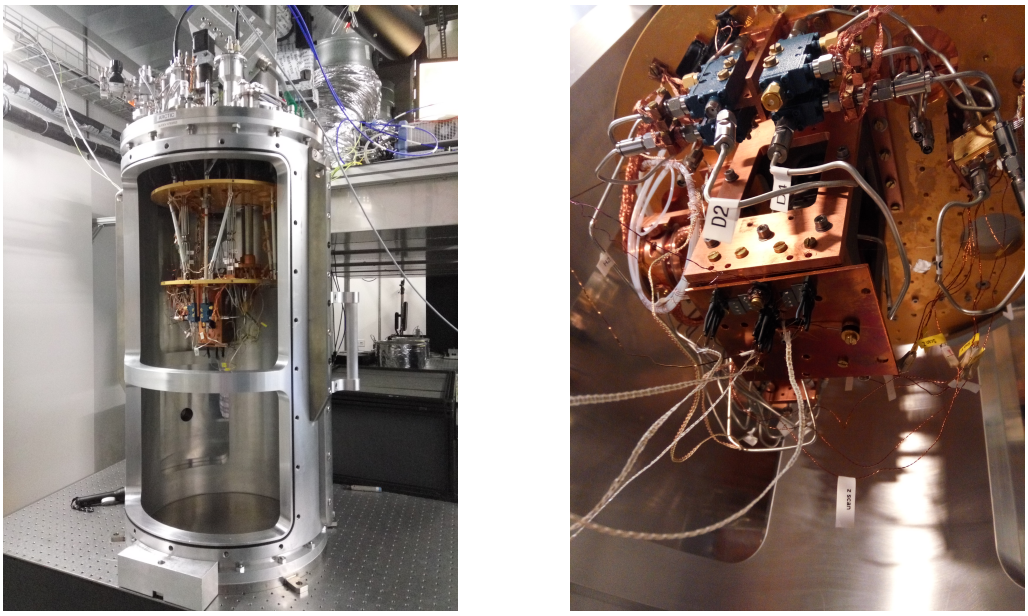

(a) (b)

Figure 4.10: (a) The home build cryogenic fridge used for measuring temperature dependent resistivity (b) The samples are mounted on the copper holder to the bottom of the bare plate at 3 K

The sample is measured in a cryogenic refrigerator which can reach temperatures below 3 K, shown in Figure 4.10a. A copper plate is used as a sample holder due to its good thermal conductivity. Four small chips (12×6 mm) are glued on this plate with GE Varnish and then bonded to four copper ports in the Printed Circuit Board (PCB) glued nearby. On the PCB, a four-pin connector is soldered onto the PCB for DC connection. The outer two ports are used as current source line and the inner ports are used to sense the voltage drop. The four-wire setup minimizes the influence of the resistance of wires and the contact resistance between sample surface and the wires.

After the samples are attached on a plate, see in Figure 4.11, the whole plate is mounted on the bottom part of the fridge indicated in Figure 4.10b. The plate is fixed to the botton part with two 3 mm screws. The distance is 2 mm. Together with the plate, a temperature sensor and a heater are mounted next to the samples with brass screws. Then the fridge is closed and cooled down to 3 K. When the fridge is cold, the heater is used to sweep the temperature between 3 K to 11 K. which is suitable for our measurement because the T_c of Nb is exactly in this interval. Since the glue GE Varnish also has a good thermal conductivity, we can assume the sample is able to finish the heat exchange with the plate in a short amount of time.

The measurement is done with a Labview program which has been written to control the temperature, wait for stabilization (120 s) and perform the resistance measurement. The four-probe measurement is done with a Keithley 2450 SourceMeter. In the source meter, an electrical current of 0.03 A has been chosen low enough not to heat the sample and large enough to give sufficient Signal-to-Noise Ratio (SNR) in the given integration window.

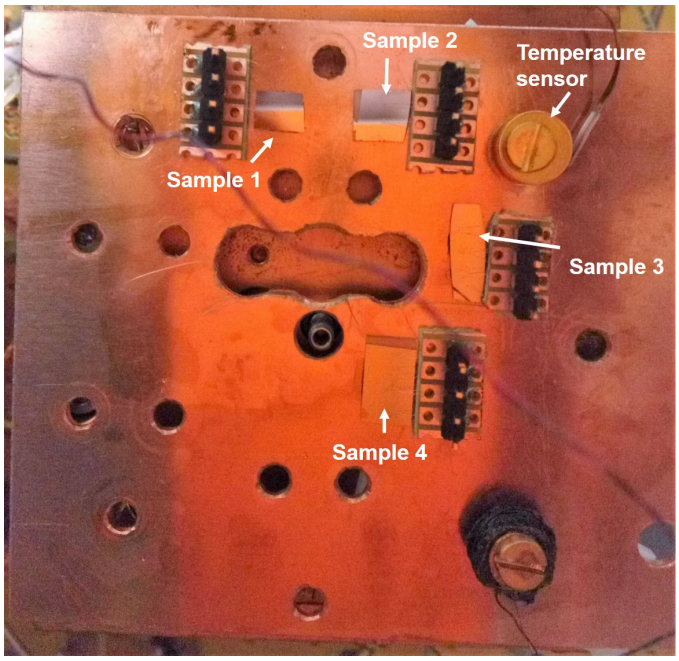

Figure 4.11: Four samples glued on a copper plate together with screw tightened heater and temperature sensor

Chapter 5

Deposition Results

Sputtering parameters were optimized by performing three studies: Deposition rate, where film properties from three different deposition rates were compared, RF bias study, where five different RF bias powers from 0 W to 50 W were compared and substrate temperature study, where deposition at six different temperatures was investigated. In all three sutdies we started from the default system parameters (Table 5.1) and vary a specific one, corresponding to the study.

Table 5.1: Standard deposition parameters

Process Parameters	
Target-Substrate Distance (mm)	130
Target Power (W)	650
Ar Pressure (mTorr)	2
Deposition Rate (nm/s)	0.85
Pre-sputtering (min)	2
Deposition Time for 150 nm (s)	174
Substrate Temperature (°C)	25

5.1 Deposition Rate Study

The deposition rate is influenced by target power, substrate-target distance and Ar pressure (see Section 3.3). Here, three sets of parameters have been chosen to study how they affect deposition rate and film quality, see Table 5.2.

In each test, a series of depositions with different coating time have been done. The approach for determining the target thickness is discussed in detail in Section 4.3 and Appendix B.3. The results of deposition rate and time for target thickness are listed in Table 5.2.

Once the the deposition time for the target thickness is obtained, two more deposition tests with the determined time are done for further characterization. One deposition is done with small chip to measure thickness and T_c and another one is done on a wafer to study stress and uniformity. All compared samples have the same thickness. Figure 5.1 shows all the characterization results for deposition rate study, in terms of surface roughness, T_c, stress and uniformity, where the deposition rate is the only changing parameter.

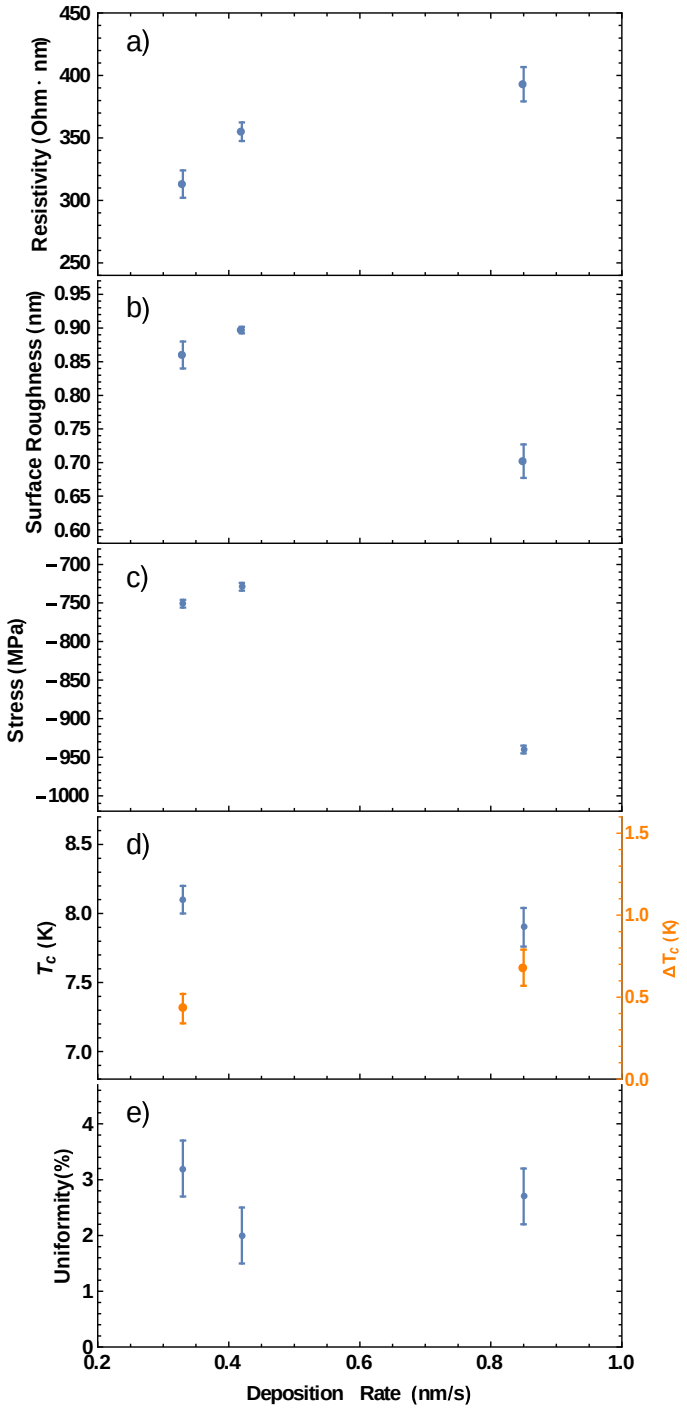

Figure 5.1: (a) The resistivity, (b) surface roughness, (c) stress, (d) T_c and ΔT_c, (e) uniformity as a function of deposition rate, where the negative value in stress represents the compressive stress.

Table 5.2: Parameters for deposition rate study

Process Parameters	Test 1	Test 2	Test 3
Target-Substrate Distance (mm)	130	180	130
Target Power (W)	650	650	250
Ar Pressure (mTorr)	2		
Substrate Temperature	Room Temperature (25 °C)		
Pre-sputtering (min)	0		
RF bias (W)	0		
Deposition Rate (nm/s)	0.85	0.42	0.35
Coating Time for 150 nm (s)	174	333	454

The resistivity increases when the deposition rate is increasing. We note that no pre-sputtering was performed for this test. The impurities in the metal target can be therefore trapped in the deposited film. For the deposition with lower rate, a longer time is needed and most of the impurities can be sputtered away during the process so that the film will be relatively pure compared to the one with higher deposition rate. To ensure the high purity and reproducibility, a pre-sputtering step is necessary. From the T_c results, we can also see that sample deposited with the highest rate shows a relatively low T_c compared to the low rate experiments. However, T_c is considerably lower than bulk value, most probable due to impurities from the target. In addition, films deposited with higher deposition rate shows higher ΔT_c, which means films are less homogeneous when the deposition rate is high. By reducing the deposition rate, one can obtain more homogeneous films.

The surface topography has been obtained by AFM for the small chips, see Figure C.1 in Appendix C. From the image, all results of surface roughness are very high compared with epi-ready substrate (RMS less than 0.2 nm).

The results of film stress are compressive (negative value) and the highest deposition rate shows the highest stress. For the two tests with lower deposition rate, the stress measurements are comparable. High rate will not provide enough time for atoms to arrange and release the stress in the lattice, so the stress is higher than the ones of Test 2 and 3. Our results are consistent with the results in [24], where low Ar pressure results in high compressive stress.

The 2-inch uniformity results of all the deposition rates are below 5%. Test 2 (Deposition rate 0.42 nm/s) has the best uniformity, due to the larger substrate-target distance than the other two experiments.

For the other studies, we have chosen the highest deposition rate considering the shortest deposition time so that the film will get least contaminants from the environment.

5.2 RF Bias Study

In this study we are interested in how RF bias affects the film properties. The RF source in the sputtering machine allows a maximum bias of substrate up to 50 W. The RF bias is varied from 0 W to 50 W, as shown in Table 5.3.

As mentioned in Section 3.3.3, RF bias can result in a more dense film and weak etching of deposited film. A small bias (10 W) is already able to reduce the thickness

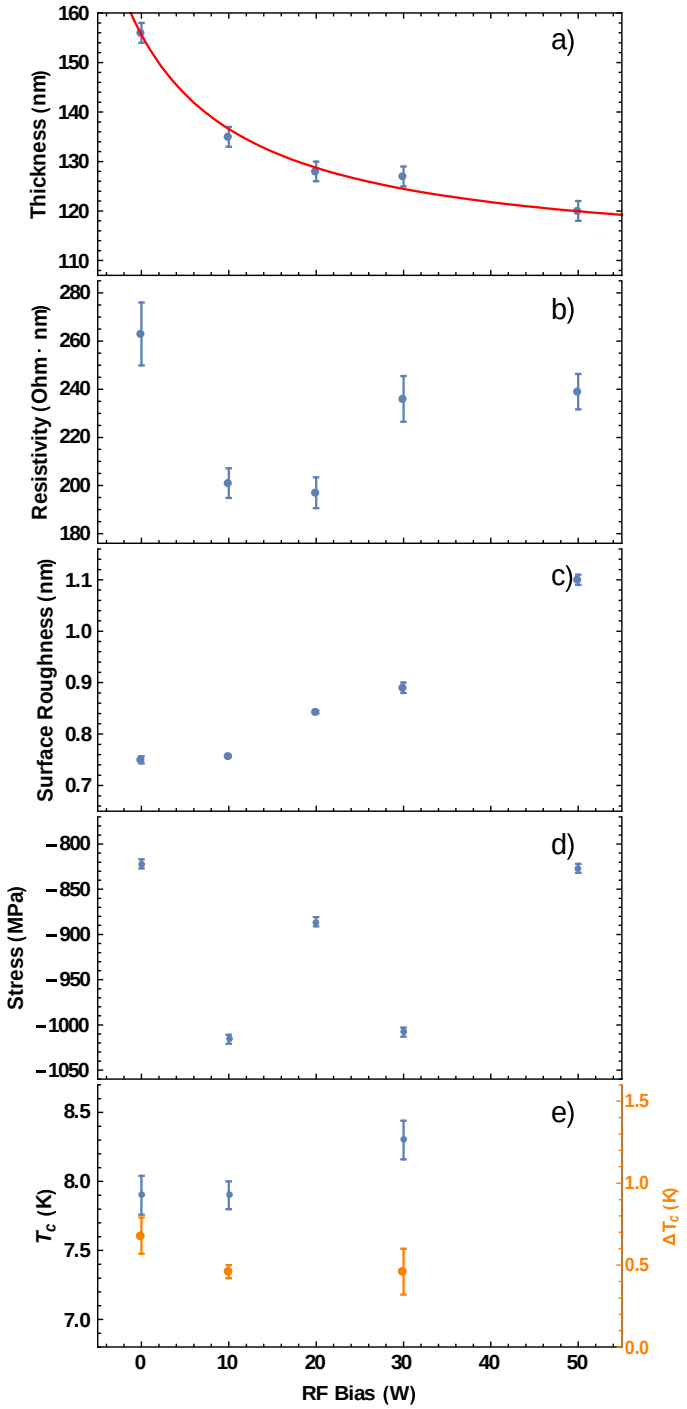

Figure 5.2: (a) The thickness, (b) resistivity, (c)surface roughness, (d) stress, (e) T_c and ΔT_c, as a function of RF bias power. Blue dots are the measured data and red line is the fitted curve.

Table 5.3: Deposition parameters for RF bias study

Process Parameters	Test 1
Target-SubstrateDistance (mm)	130
Target Power (W)	650
Ar Pressure (mTorr)	2
Substrate Temperature	Room Temperature (20 °C)
Deposition Rate (nm/s)	0.85
Coating Time (s)	174
RF bias (W)	0 - 50

by 20 nm. When the bias increases, the reduction of thickness tends to saturate, where the bias dependent thickness can be fitted by a inverse proportion function (red line in Figure 5.2a).

The resistivity reduces with lower bias power. When the bias is larger than 30 W, the resistivity increases again. Low resistivity can be associated with denser films and lower impurity content. Small bias can repel the oxygen impurities from the films and helps to purify the film [31]. However, large bias will destroy the crystal structure of the film. Both of the effects will influence the resistivity of the film, so there is a trade-off and an optimal point to obtain the lowest resistivity in terms of the choice of RF bias power.

RF bias is also known to affect the stress of the film [24]. Our results have shown a high compressive stress of the deposited films (See Figure 5.2d). However, there is no obvious correlation between the applied power and the stress in the film, even if the variation of stress can reach up to 200 MPa with different RF bias power. This is in agreement with the results in [24], where RF bias results in compressive stress.

The influence of large bias is also reflected from AFM images and surface roughness. When the applied power increases the increase of roughness can be observed and the results can be fitted by a parabolic function (See Figure 5.2c and 5.3). Samples deposited at 10 W and 50 W have shown different surface topography. One can see the small bumps incorporated in the film at a power of 50 W, resulting in a large surface roughness, probable due to disturbance of crystal growth from the Ar ion bombardment. Therefore the deposition with high RF bias should be avoided.

We have also observed the increase of T_c and decrease of ΔT_c with the increase of RF bias since the impurities in the film can be partially removed and the films are more homogeneous.

As a result, small bias (less than 20 W) helps reduce the impurity level inside the deposited films without damaging the crystal formation of Nb, which can be used in the deposition process to get better films.

5.3 Temperature Study

In this section we discuss the temperature study results when the substrate temperature is varied from room temperature (25°C) to 1000°C with other parameters kept the same (See Table 5.4).

The deposition is done for both small samples and 2-inch wafers. We note that in this study we use sapphire wafers. Since different substrates can lead to different

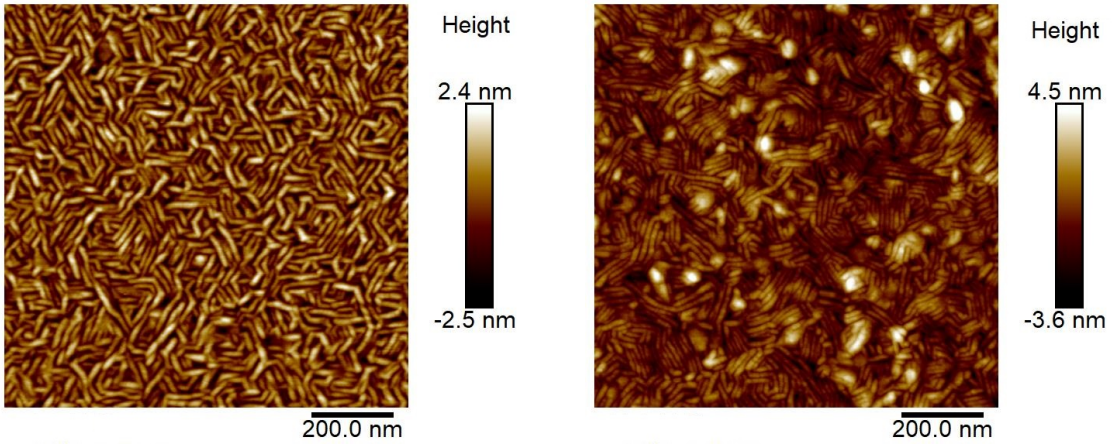

(a) 10 W (b) 50 W

Figure 5.3: Comparison of AFM images for sample deposited with RF bias power of (a) 10 W and (b) 30 W.

deposition results, it is important to develop a deposition process for the same substrate as is used for superconducting circuits. However, using sapphire wafer, we will be unable to measure stress as discussed in Section 4.4.

Table 5.4: Deposition parameters for RF bias study

Process Parameters	Test 1
Target-SubstrateDistance (mm)	130
Target Power (W)	650
Ar Pressure (mTorr)	2
RF bias (W)	0
Deposition Rate (nm/s)	0.85
Coating Time (s)	174
Substrate Temperature (°C)	25 - 1000

The thickness of films deposited during this study varies from 145 to 152 nm. We can conclude that film thickness is not affected by substrate temperature during the process.

The resistivity decreases with increasing temperature, with a small step at 600°C, above which the resistivity is approximately constant (See Figure 5.4a). At high temperatures Nb atoms move and form larger grains and better crystal structure. This is reflected by lower resistivity of films deposited at temperature above 600°C.

Apart from resistivity, T_c and RRR provide additional means to investigate the impurities and defect level in the samples. The T_c and RRR results (Figure 5.4c) are consistent. Nb with higher T_c also has high RRR. The maximum values are obtained for the film deposited at 600°C (T_c 9.34 K, which is close to the bulk value). The RRR of this film is one order of magnitude higher than the film deposited at 25°C and 4 times larger than the other films deposited with high temperature, which is best among all the films we have deposited.

Temperature also changes surface topography of deposited films (See Figure 5.5). Higher temperature results in larger grain size, and therefore increases the roughness. Larger grain size has smaller surface-to-volume ratio, which leads to reduced chance

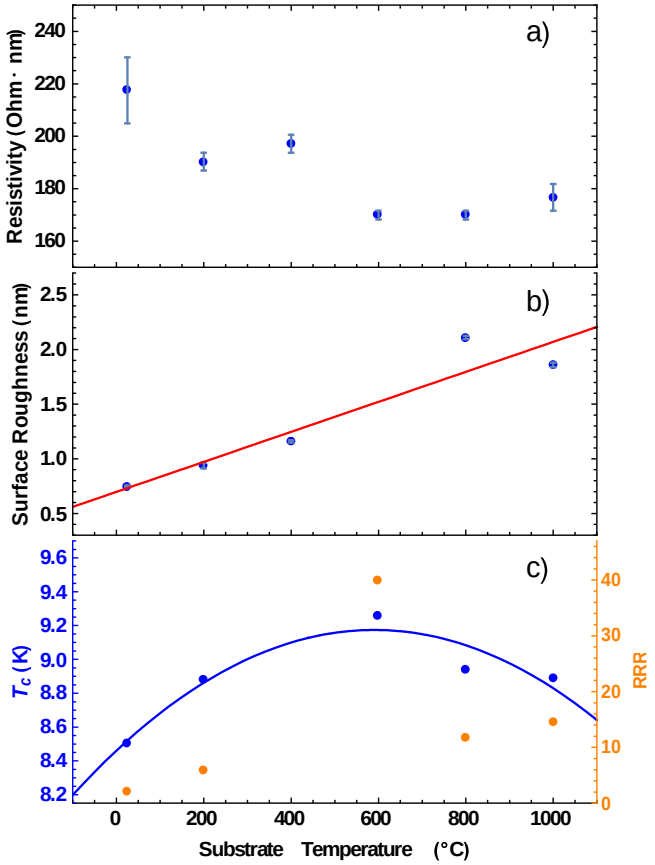

Figure 5.4: (a) The resistivity , (b) surface roughness, (c) T_c and RRR as a function of substrate temperature, where the blue solid curve is a fitted parabolic function.

of surface contamination, and reduced number of weak links between the grain.

At even higher temperatures ($T \geq 800°C$) the T_c and RRR decrease probably due to oxidation of Nb at the metal-substrate boundary [32].

The best Nb film according to our characterization is obtained at deposition temperature of 600°C.

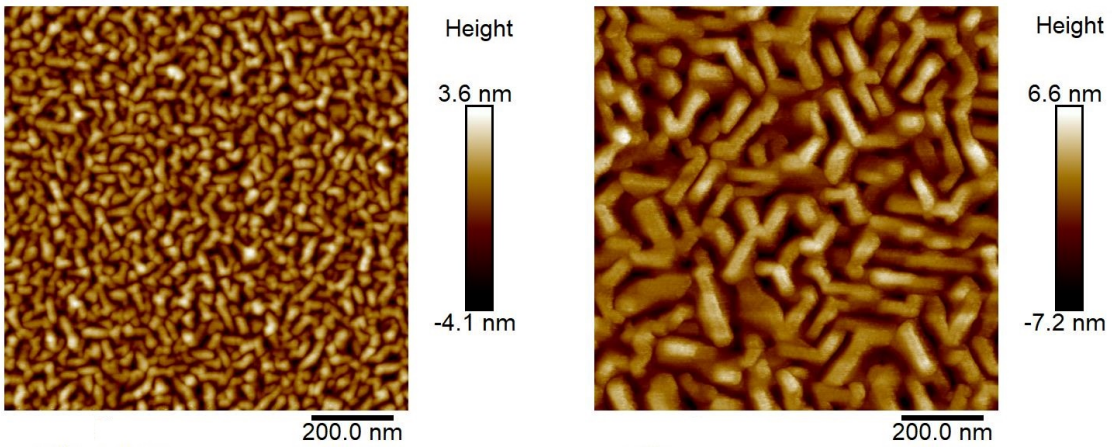

(a) 200°C (b) 800°C

Figure 5.5: AFM images of small chips deposited at (a) 200°C and (b) 800°C.

Chapter 6

Conclusions

In this thesis a detailed investigation of Nb deposition has been conducted using the AJA sputtering system. The process has been successfully calibrated for reaching a good quality Nb thin film. Effects of deposition rate, RF bias power and substrate temperature have been studied. Their influence on the thin film properties, in terms of resistivity, thickness, topography, surface roughness, stress, critical temperature and temperature dependent resistivity is investigated.

Deposition rate study shows that the highest deposition rate results in the highest stress, and that uniformity improves with higher substrate-target distance. RF bias study shows that T_c increases with the increase of RF bias. Small bias (less than 20 W) helps reduce the impurity level inside the deposited films without damaging the crystal formation of Nb, which can be used in the deposition process to get better films. Deposition temperature study shows that there is an optimal deposition temperature (600°C). Films deposited in this way shows the highest T_c and RRR.

Our study shows that best films are obtained with the following parameters: a target power of 650 W, a substrate-target distance of 130 mm, zero RF bias, a substrate temperature of 600 °C and an Ar pressure of 2 mTorr. Our best films have a superconducting transition temperature of 9.34 K and a residual resistivity ration (RRR) of 40.

In order to fabricate high quality resonators, a good Nb thin film is only the first step. Next steps could include optimization of additional parameters such as Ar pressure, temperature study with low deposition rate and finally wafer cleaning.

Appendix A

Fabrication Process for Superconducting Circuits

A.1 Overview of the Fabrication for Lumped-element Resonators

The fabrication of superconducting circuits is done by exploiting a series of techniques, which are widely used in the microelectronics field, including lithography (optical or electron beam), deposition (sputtering) etching (reactive ion etching) and cleaning procedures.

In this thesis, the substrate used for testing Nb sputtering and resonator is epi-ready (RMS roughness less than 0.2 nm) sapphire wafer from Rubicon. The resonator is patterned on the Nb with one photolithography process (one mask). The full process flow can be summarized into five major steps and the schematic can be seen in Figure A.1. Firstly, the substrate is cleaned to obtain a clean surface. Then the metal deposition will be performed, which is the major work in this thesis. Once we have a thin film metal on the substrate, a layer of polymer called photo resist is spin coated on the metal and photolithography process is used to create a pattern based on the design on the mask. Next, an etching process is used to create the pattern onto the metal film. Finally the chip with a resonator is done after stripping the photo resist. The work in this thesis will focus on the metal deposition process and obtain the optimal deposition parameters and film quality.

A.2 Recipes for Substrate Cleaning and Nb Deposition

The following recipe was used to produce 150 nm thick Nb films on 2-inch sapphire substrate which yielded Q-loaded of a lumped element resonator at low photon numbers of 280 k.

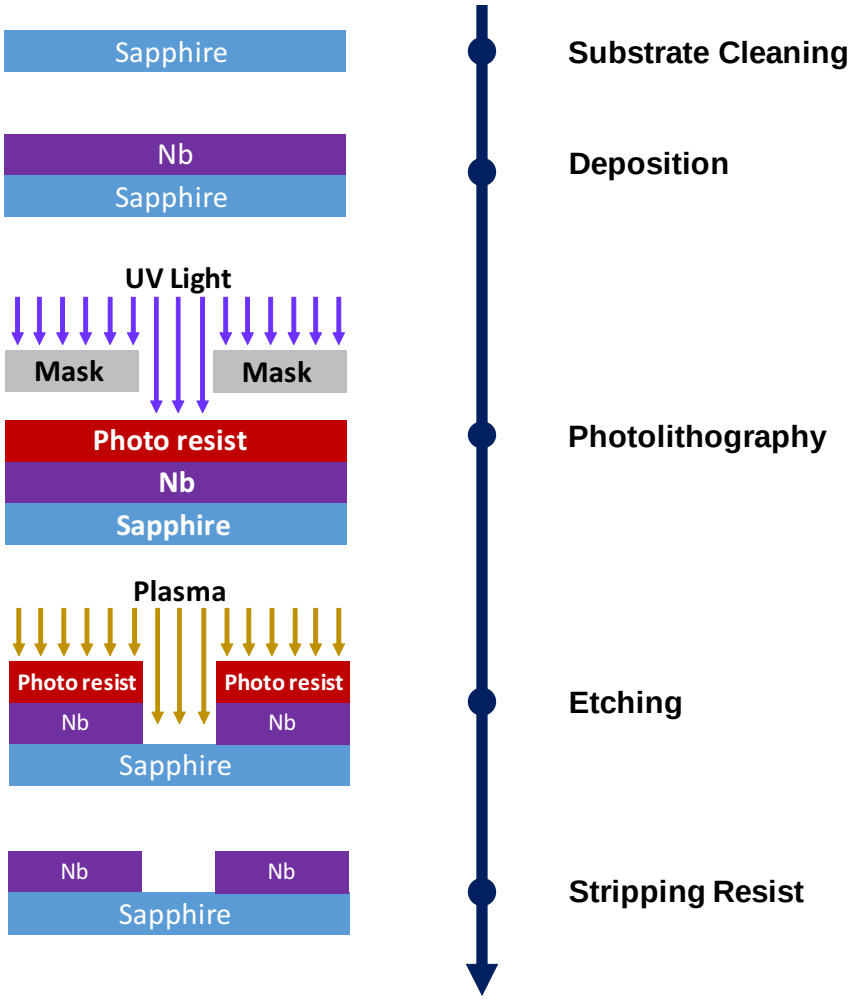

Figure A.1: The schematic of process flow for fabricating lumped element resonator.

Table A.1: Substrate cleaning and deposition recipe

Substrate Cleaning
Acetone in 50°C ultrasonic bath with power 4
Isopropanol in 50°C ultrasonic bath with power 4
Water rince for 2 min
Pirahna (H_2SO_4:H_2O_2 = 4:1) 10 min
Water rince for 5 min
Water spinner 1500 rpm 500 s with DI water
Water spinner 3000 rpm 150 s dry
Nb sputtering
Load sample holder in load lock
Pump down load lock until pressure below 1×10^{-6} Torr
Transfer the sample holder to UHV chamber
Adjust height to 100 mm (Substrate-target distance 130 mm)
Close cryopump valve
Turn on rotation with 40 rpm
Ramp up the temperature to 900°C by 2°C/s
Open cryopump valve
Wait for 1 hour
Ramp down to 600°C by 2°C/s
Wait for 30 min
Close cryopump valve
Turn on Ar gas with a flow of 30 sccm
Adjust pressure of Ar to 3 mTorr
Ignite plasma with 50 W target power
Reduce the Ar pressure to 2 mTorr Ramp up target power to 650 W in 2 min
Wait for 2 min
Open target shutter
Coating time 174 s
Close target shutter
Ramp down target power to 50 W in 2 min
Turn off power and Ar gas
Open all the pumps
Ramp down substrate temperature to 60°C by 2°C/s

Appendix B

Thickness Measurement

B.1 Lift-off Method

To measure the thickness, the sample is first mounted on a piece of glass and a tip inside the machine will scan along the surface. The profile measured from DektakXT is shown in Figure B.1. To eliminate the influence of tilted effect from the environment, a leveling operation is done by placing the red cursor and green cursor to the left and right edge of trench. Then the two edges of the trench are on the same level. Both of the cursors can be expanded and the average height value will be taken for expanded cursor. The thickness can be obtained by calculating the height difference after placing two cursors in the trench and on the metal stair respectively.

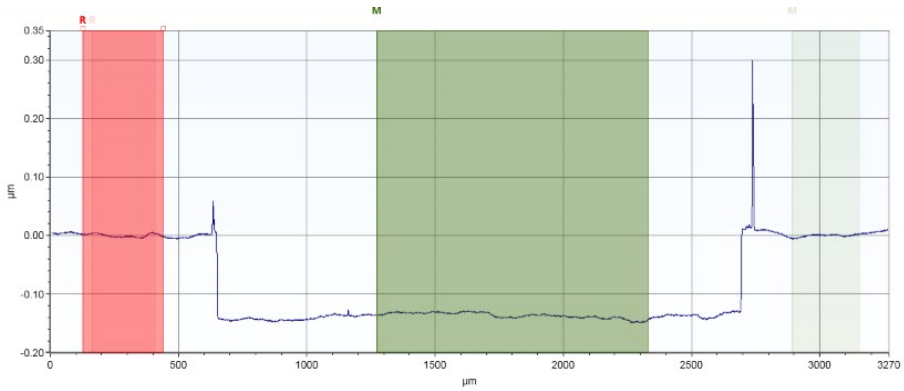

Figure B.1: The thickness measurement profile, where the spike comes from the lift-off. The height difference between the average of red marker range and green marker range is calculated as the step thickness.

B.2 Etching Method

The profile from the etching method for measuring thickness is shown in Figure B.2. The yellow part is Nb step and brown part is the trench. The slope in the figure comes from the AFM measurement artefact. The thickness can be obtained from the height difference of two cursors. The error (3 nm) introduced by this method is acceptable for our experiments.

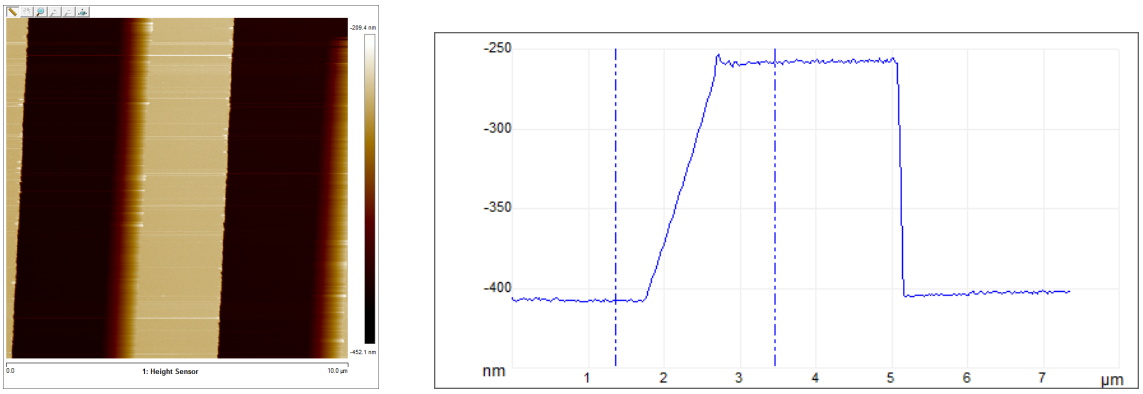

(a) (b)

Figure B.2: (a)AFM topography ($10\mu m \times 10\mu m$) of the trench after photolithography and dry etching. The yellow part is Nb stair and red ones are the sapphire trench. The slope of Nb left edge is the AFM measurement artefact from trace and retrace. (b)The thickness measurement shows a step with 150 ± 2 nm thick

B.3 Determination of Target Thickness

Our target thickness is 150 nm. The target thickness should be high enough to ensure the thin film is larger than London penetration depth. The London magnetic penetration depth of Nb has be expressed by equation 2.1. When thickness is above 100 nm, the T_c is approaching the bulk value [33]. On the other hand, the thickness should not be too high to influence subsequent fabrication processes, such as the contact between Al and Nb, as shown in Figure B.3.

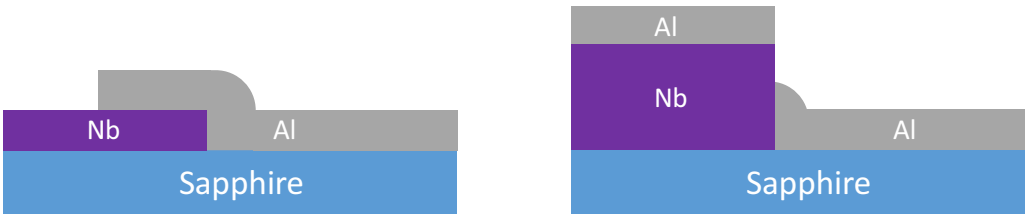

(a) (b)

Figure B.3: The schematic for an example of Nb-Al contact. If the thickness of Nb is too large, the connection between evaporated Al parts on Nb will result in discontinuities. (a) The evaporated Al has good step coverage on thinner Nb (b) Bad step coverage for thick Nb film

The method for the measurement of thickness in deposition rate study is lift-off and Dektak as mentioned in Section 4.3. For each set of process parameters, we only vary the deposition time and measure the thickness of deposited samples. Based on the measured thickness, a linear function is fitted and the extracted slope is the deposition rate. The results of Test 1 is shown in Figure B.4

From deposition rate, the deposition time needed for target thickness (150 nm) can also be known. By using the same approach, the deposition rate and time for target thickness can also be obtained for Test 2 and Test 3.

For the test with lower deposition rate (Test 2 and Test 3 in Table 5.2), the extracted coating time have fitted well with the prediction. But for the highest rate

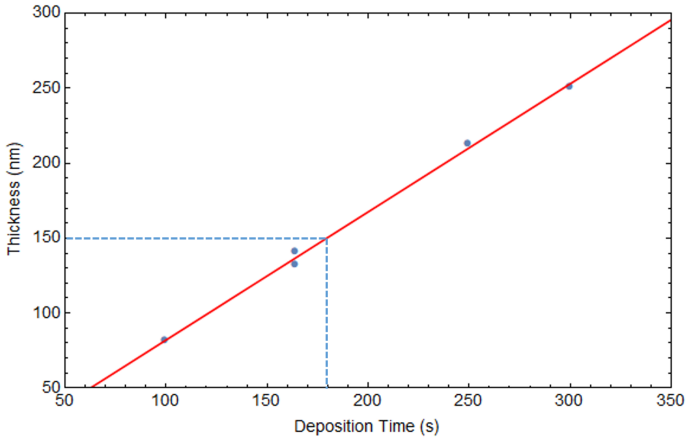

Figure B.4: Film thickness as a function of deposition time for the Test 1. Blue dots are the measured data and red solid line is the fitted linear function

(Test 1), a more than 10 % offset of thickness has been observed. To compensate this offset, the coating time have been reduced by 5 s. The final coating time for Test 1 is 174 s and the results for thickness are good for further tests. All the results of deposition rate and time for target thickness are listed in Table 5.2.

Appendix C

AFM Measurement

C.1 Deposition Rate Study

For the deposition at room temperature without any bias, the topography looks similar, where the polycrystalline structure shows a "worm like" surface. All the AFM images have been taken with a range of $1\mu m \times 1\mu m$. The grain size is around 40 nm. The calculated surface roughness for each AFM image is plotted in Figure 5.1. They have shown similar results which is consistent with the topography and the grain size we have seen from the image.

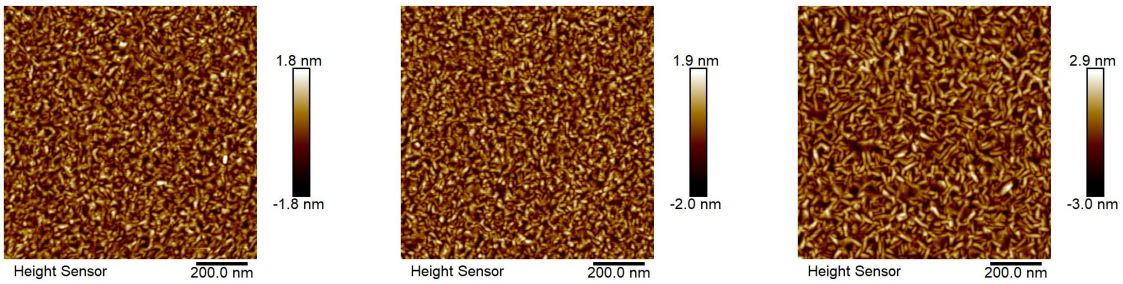

(a) 0.85 nm/s (b) 0.42 nm/s (c) 0.35 nm/s

Figure C.1: The AFM surface topography of samples deposited at different rate

Bibliography

[1] S. L. Braunstein and P. van Loock, "Quantum information with continuous variables," vol. 77, no. 2, pp. 513–577.

[2] R. Blatt and D. Wineland, "Entangled states of trapped atomic ions," vol. 453, no. 7198, pp. 1008–15.

[3] N. A. Gershenfeld and I. L. Chuang, "Bulk spin-resonance quantum computation," vol. 275, no. 5298, pp. 350–356.

[4] R. Hanson, L. P. Kouwenhoven, J. R. Petta, S. Tarucha, and L. M. K. Vandersypen, "Spins in few-electron quantum dots," vol. 79, no. 4, pp. 1217–1265.

[5] Y. Nakamura, Y. A. Pashkin, and J. S. Tsai, "Coherent control of macroscopic quantum states in a single-cooper-pair box," vol. 398, no. 6730, pp. 786–788.

[6] T. D. Ladd, F. Jelezko, R. Laflamme, Y. Nakamura, C. Monroe, and J. L. O'Brien, "Quantum computers," *Nature*, vol. 464, pp. 45–53, 2010.

[7] M. H. Devoret, A. Wallraff, and J. M. Martinis, "Superconducting qubits: A short review,"

[8] M. Tinkham, *Introduction to Superconductivity*. Dover Publications, 2004.

[9] B. D. Josephson, "Supercurrents through barriers," vol. 14, no. 56, pp. 419–451.

[10] M. H. Devoret and R. J. Schoelkopf, "Superconducting circuits for quantum information: an outlook," *Science*, vol. 339, no. 6124, pp. 1169–1174, 2013.

[11] C. Wang, C. Axline, Y. Y. Gao, T. Brecht, Y. Chu, L. Frunzio, M. Devoret, and R. Schoelkopf, "Surface participation and dielectric loss in superconducting qubits," *Applied Physics Letters*, vol. 107, no. 16, p. 162601, 2015.

[12] A. Blais, R.-S. Huang, A. Wallraff, S. M. Girvin, and R. J. Schoelkopf, "Cavity quantum electrodynamics for superconducting electrical circuits: An architecture for quantum computation," vol. 69, no. 6, p. 062320.

[13] P. K. Day, H. G. LeDuc, B. A. Mazin, A. Vayonakis, and J. Zmuidzinas, "A broadband superconducting detector suitable for use in large arrays," vol. 425, no. 6960, pp. 817–821.

[14] A. Megrant, C. Neill, R. Barends, B. Chiaro, Y. Chen, L. Feigl, J. Kelly, E. Lucero, M. Mariantoni, P. J. J. O'Malley, D. Sank, A. Vainsencher, J. Wenner, T. C. White, Y. Yin, J. Zhao, C. J. Palmstrom, J. M. Martinis, and A. N.

Cleland, "Planar superconducting resonators with internal quality factors above one million," vol. 100, no. 11, p. 113510.

[15] J. Wenner, R. Barends, R. C. Bialczak, Y. Chen, J. Kelly, E. Lucero, M. Mariantoni, A. Megrant, P. J. J. O'Malley, D. Sank, A. Vainsencher, H. Wang, T. C. White, Y. Yin, J. Zhao, A. N. Cleland, and J. M. Martinis, "Surface loss simulations of superconducting coplanar waveguide resonators," vol. 99, no. 11, p. 113513.

[16] R. A. Kamper, "Superconducting materials," in *Electronics Design Materials*, Palgrave Macmillan UK, 1971.

[17] H. K. Onnes, "The resistance of pure mercury at helium temperatures," *Commun. Phys. Lab. Univ. Leiden*, vol. 12, no. 120, p. 1, 1911.

[18] J. Bardeen, L. N. Cooper, and J. R. Schrieffer, "Theory of superconductivity," *Physical Review*, vol. 108, no. 5, p. 1175, 1957.

[19] W. Meissner and R. Ochsenfeld, "Ein neuer effekt bei eintritt der supraleitfähigkeit," *Naturwissenschaften*, vol. 21, no. 44, pp. 787–788, 1933.

[20] F. London and H. London, "The electromagnetic equations of the supraconductor," in *Proceedings of the Royal Society of London A: Mathematical, Physical and Engineering Sciences*, vol. 149, pp. 71–88, The Royal Society, 1935.

[21] "Principles of magnetron sputtering." http://nabis.fisi.polimi.it/equipments/aja-atc-orion-8-sputtering-system/. Accessed: 2017-08-31.

[22] X. Meng, X. Fan, and H. Guo, "A new formula on the thickness of films deposited by planar and cylindrical magnetron sputtering," *Thin Solid Films*, vol. 335, no. 1, pp. 279–283, 1998.

[23] S. Swann, "Magnetron sputtering," *Physics in technology*, vol. 19, no. 2, p. 67, 1988.

[24] T. Imamura, S. Ohara, and S. Hasuo, "Bias-sputtered nb for reliable wirings in josephson circuits," vol. 27, no. 2, pp. 3176–3179.

[25] T. Imamura and S. Hasuo, "Effects of intrinsic stress on submicrometer nb/alo/-sub x//nb josephson junctions," *IEEE transactions on magnetics*, vol. 25, no. 2, pp. 1119–1122, 1989.

[26] G.-i. Oya, M. Koishi, and Y. Sawada, "High-quality single-crystal nb films and influences of substrates on the epitaxial growth," vol. 60, no. 4, pp. 1440–1446.

[27] F. M. Smits, "Measurement of sheet resistivities with the four-point probe," vol. 37, no. 3, pp. 711–718.

[28] L. B. Valdes, "Resistivity measurements on germanium for transistors," vol. 42, no. 2, pp. 420–427.

[29] G. Binnig, C. F. Quate, and C. Gerber, "Atomic force microscope," vol. 56, no. 9, pp. 930–933.

[30] M. Krishnan, E. Valderrama, B. Bures, K. Wilson-Elliott, X. Zhao, L. Phillips, A.-M. Valente-Feliciano, J Spradlin, C. Reece, and K. Seo, "Very high residual resistivity ratios of heteroepitaxial superconducting niobium films on MgO substrates," vol. 24, no. 11, p. 115002.

[31] "Aja tutorial." http://www.ajaint.com/substrate-holders.html. Accessed: 2017-08-31.

[32] C. Sürgers and H. v. Löhneysen, "Effect of oxygen segregation on the surface structure of single-crystalline niobium films on sapphire," *Applied Physics A*, vol. 54, no. 4, pp. 350–354, 1992.

[33] A. I. Gubin, K. S. Il'in, S. A. Vitusevich, M. Siegel, and N. Klein, "Dependence of magnetic penetration depth on the thickness of superconducting nb thin films," vol. 72, no. 6, p. 064503.

Eidgenössische Technische Hochschule Zürich
Swiss Federal Institute of Technology Zurich

Declaration of originality

The signed declaration of originality is a component of every semester paper, Bachelor's thesis, Master's thesis and any other degree paper undertaken during the course of studies, including the respective electronic versions.

Lecturers may also require a declaration of originality for other written papers compiled for their courses.

I hereby confirm that I am the sole author of the written work here enclosed and that I have compiled it in my own words. Parts excepted are corrections of form and content by the supervisor.

Title of work (in block letters):

Sputtering Process Development for High Quality Nb Thin Film

Authored by (in block letters):

For papers written by groups the names of all authors are required.

Name(s):	**First name(s):**
Wang	Zhiren

With my signature I confirm that

- I have committed none of the forms of plagiarism described in the 'Citation etiquette' information sheet.
- I have documented all methods, data and processes truthfully.
- I have not manipulated any data.
- I have mentioned all persons who were significant facilitators of the work.

I am aware that the work may be screened electronically for plagiarism.

Place, date	**Signature(s)**
Zurich, 05/09/2017	Zhiren Wang

For papers written by groups the names of all authors are required. Their signatures collectively guarantee the entire content of the written paper.